Electronic Supplementary Material (ESI) for Soft Matter.

Supporting Information: Nanocomposite Tectons as Unifying Systems for Nanoparticle Assembly

Jianshe Xia,[†,‡] Margaret Lee,[¶] Peter J. Santos,[¶] Nathan Horst,[§,‖] Robert J. Macfarlane,[¶] Hongxia Guo,[*,†,‡] and Alex Travesset[*,⊥]

† *Beijing National Laboratory for Molecular Sciences, Institute of Chemistry, Chinese Academy of Sciences, Beijing 100190, China*

‡*University of Chinese Academy of Sciences, Beijing 100049, China*

¶*Department of Materials Science and Engineering, Massachusetts Institute of Technology, 77 Massachusetts Avenue, Cambridge, Massachusetts 02139, United States*

§*Department of Materials Science and Engineering, Iowa State University, Ames, Iowa 50011, USA*

‖*Ames Laboratory, U.S. Department of Energy, Ames, Iowa 50011, USA*

⊥*Department of Physics and Astronomy and Department of Materials Science and Engineering, Iowa State University and Ames Lab, Ames, IA 50011, USA*

E-mail: hxguo@iccas.ac.cn; trvsst@ameslab.gov

MD Force Field Parameters

Table S1: Pairwise interaction strength of Lennard-Jones (LJ) potentials, ϵ_{ij} are summarized, with the hybridization interaction energy defined between CG particles "A" and "B" $\epsilon_H = \varepsilon_{AB}$.

ϵ_{ij}	PS	FL	A	B
PS	1	1	1	1
FL	1	1	1	1
A	1	1	1	ϵ_H
B	1	1	ϵ_H	1

Table S2: Effective LJ diameter of beads in the system, σ_{ij} are calculated by additive arithmetic rules, and summarized below.

σ_{ij}	PS	FL	A	B
PS	1	0.75	0.75	0.75
FL	0.75	0.5	0.5	0.5
A	0.75	0.5	0.5	0.5
B	0.75	0.5	0.5	0.5

Table S3: Cutoff of the non-bonded potential, with most pairwise interactions truncated at the LJ energy minimimum ($2^{1/6}\sigma_{ij}$) and extended range interactions for PS-PS and A-B interactions.

$r_{cut}(\sigma_{ij})$	PS	FL	A	B
PS	2.5	$2^{1/6}$	$2^{1/6}$	$2^{1/6}$
FL	$2^{1/6}$	$2^{1/6}$	$2^{1/6}$	$2^{1/6}$
A	$2^{1/6}$	$2^{1/6}$	$2^{1/6}$	2.5
B	$2^{1/6}$	$2^{1/6}$	2.5	$2^{1/6}$

Table S4: Harmonic bond potentials between CG beads in our system.

	PS-PS	PS-NCT	PS-Core
$r_0(\sigma)$	0.84	0.63	0.84
$k(\frac{\epsilon}{\sigma^2})$	330	330	330

Table S5: Harmonic angle potentials between CG beads in our system.

	PS-PS-PS	PS-PS-NCT	PS-PS-Core
θ_0	180	180	180
$k(\epsilon)$	k_θ	k_θ	k_θ

Solvent Quality

We set up our model to mimic NCTs in "good solvent" conditions. The solvent quality is parameterized through the coarse-grained temperature of the system. The different regimes (good, θ and poor solvent) are determined through the analysis of the polymer radius of gyration R_g for varying polymer length n – where constant $\log(\frac{<R_g^2>}{n}) \approx -1.38$ for increasing $\log(n)$ corresponds to the theta temperature (T_θ) of the system. Then, with $r_0 = 0.84$ (from the coefficient of the harmonic bond) it is

$$\langle R_g^2 \rangle \approx \frac{C_\infty n r_0^2 \sigma^2}{6} \rightarrow C_\infty \approx 2.14 \tag{S1}$$

and from

$$\left.\begin{aligned} n r_0 \sigma &= Nb \\ C_\infty n r_0^2 \sigma^2 &= Nb^2 \end{aligned}\right\} \rightarrow b = 1.79\sigma \quad , \quad N = 0.47n \ . \tag{S2}$$

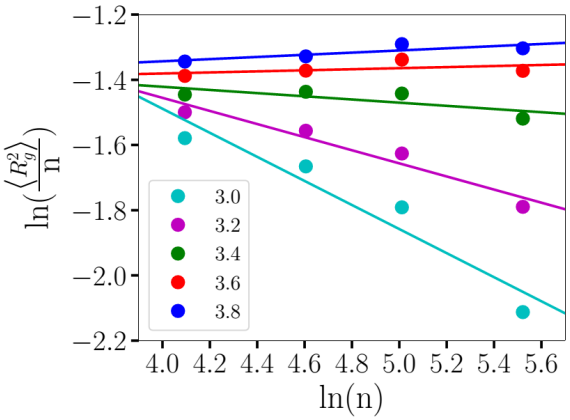

Figure S1: The variation of $\log(\frac{<R_g^2>}{\mathrm{n}})$ with ln(n), where the theta temperature $T_\theta = 3.5$.

The analysis of T_θ is shown in Fig. S1. The good solvent condition requires $T > 3.5$. Therefore, the temperature used in our simulations is $T = 4.0$. These conditions are reflected in the calculated potential of mean force, where in the absence of hydrogen bonding the potential is repulsive.

Dependence of hybridizations on core size

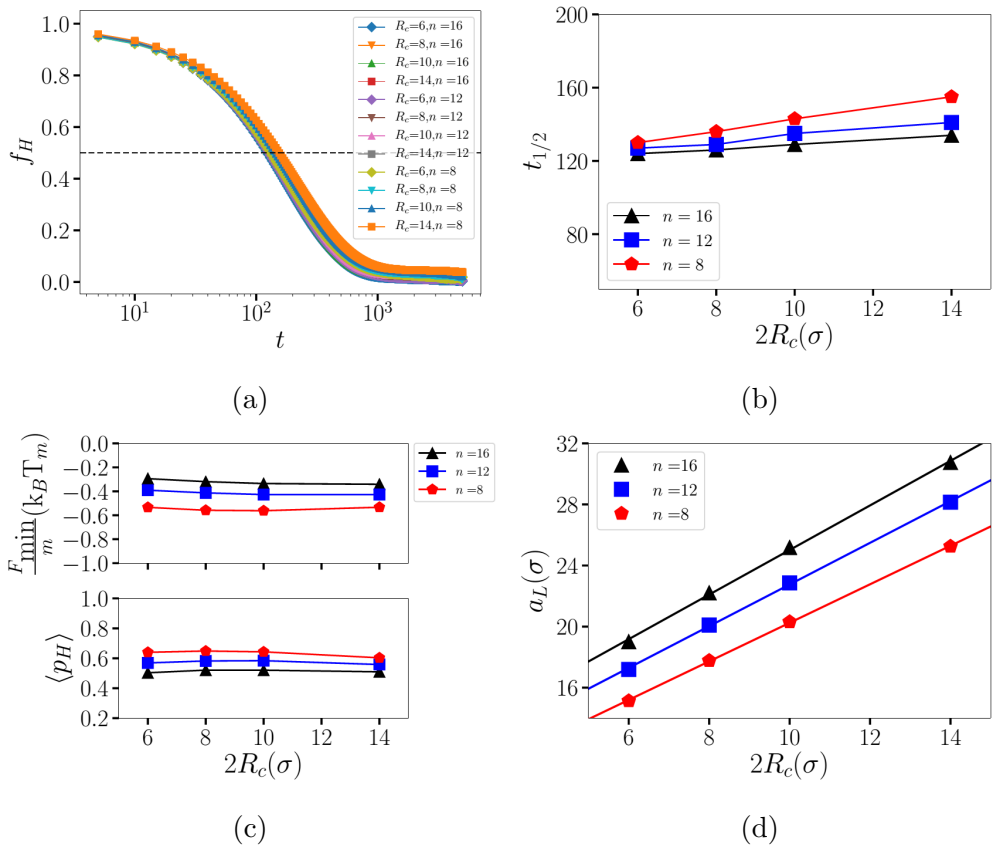

Figure S2: (a) The fraction of hybridizations f_H that lives up to a time t as a function of the core diameter $2R_c$; (b) The mean lifetime of a hybridization, (c) the minimum of the free energy per F_{min}/m and (d) the corresponding lattice constant a_L vary with $2R_c$, where a_L changes linearly with $2R_c$. All plots correspond to the CsCl lattices at $\frac{\varepsilon_{AB}}{k_BT_m} = 13.0$ with the core diameter $2R_c = 6, 8, 10, 14\sigma$, see Table 2.

Calculation of Free Energies

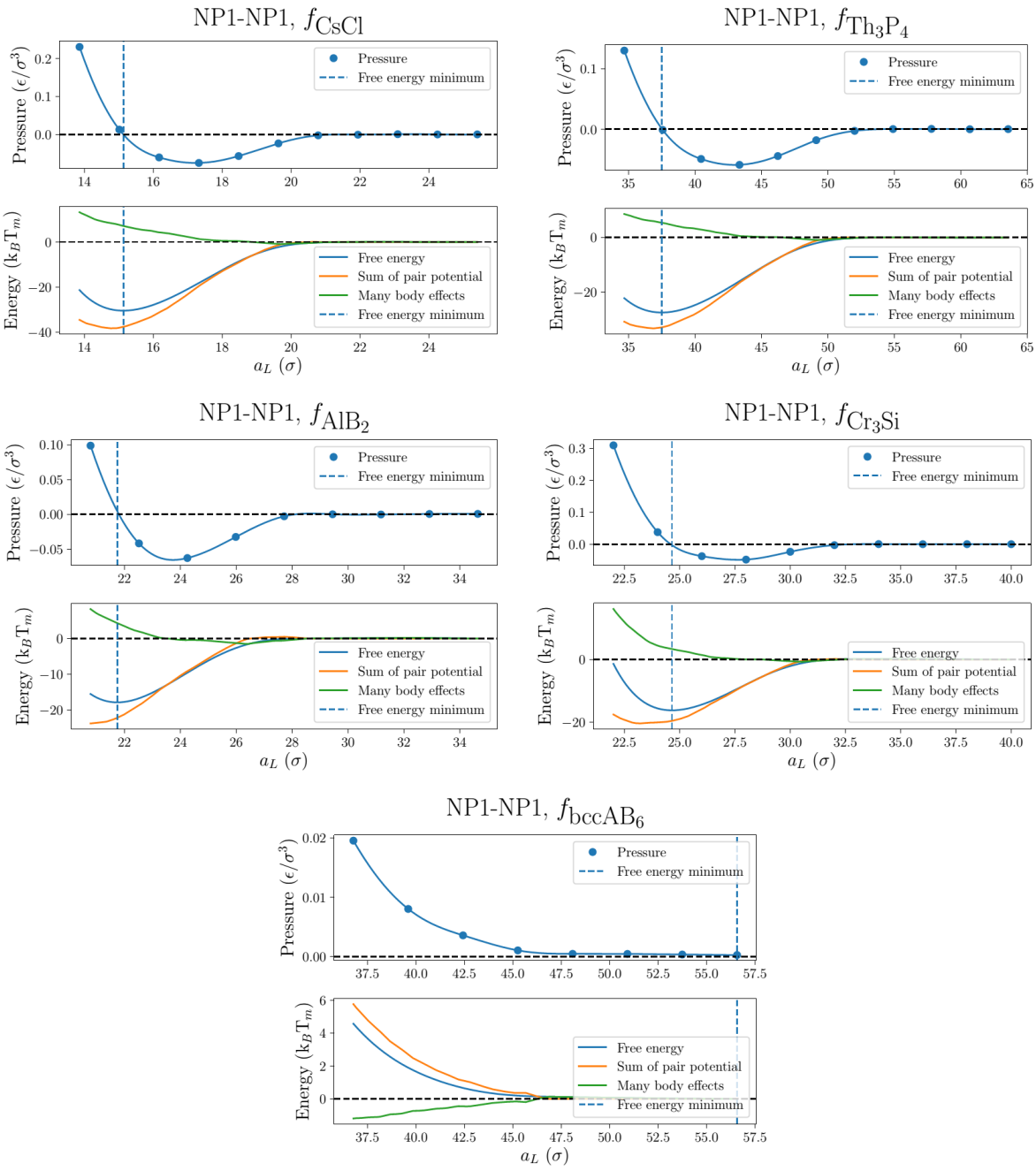

Figure S3: Pressure and free energy vs lattice constant for the BNSL CsCl, Th_3P_4, AlB_2, Cr_3Si and $bccAB_6$ with NP1 normalized to the number of NPs within the unit cell.

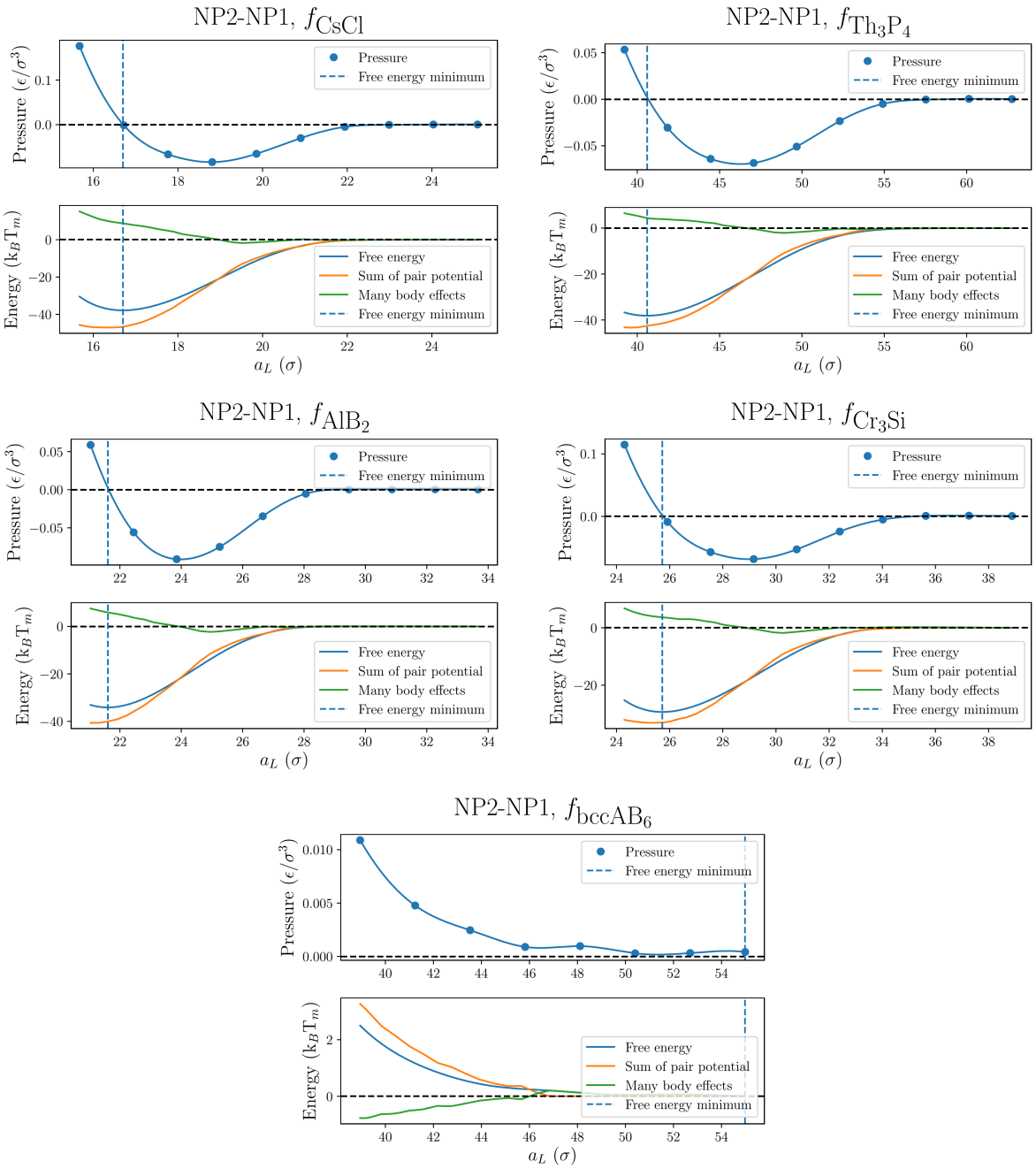

Figure S4: Pressure and free energy vs lattice constant for the BNSL CsCl, Th_3P_4, AlB_2, Cr_3Si and $bccAB_6$ with NP1 and NP2 normalized to the number of NPs within the unit cell.

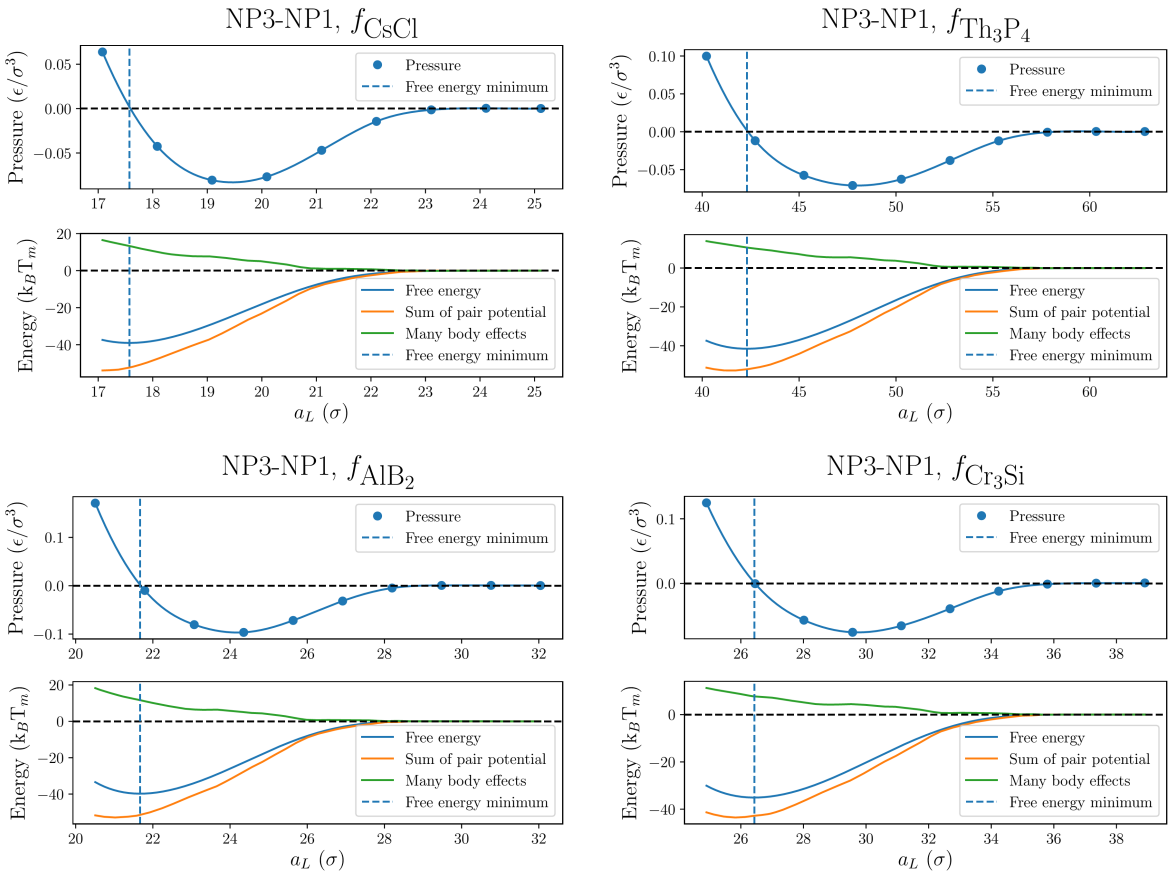

Figure S5: Pressure and free energy vs lattice constant for the BNSL CsCl, Th_3P_4, AlB_2, and Cr_3Si with NP1 and NP3 normalized to the number of NPs within the unit cell.

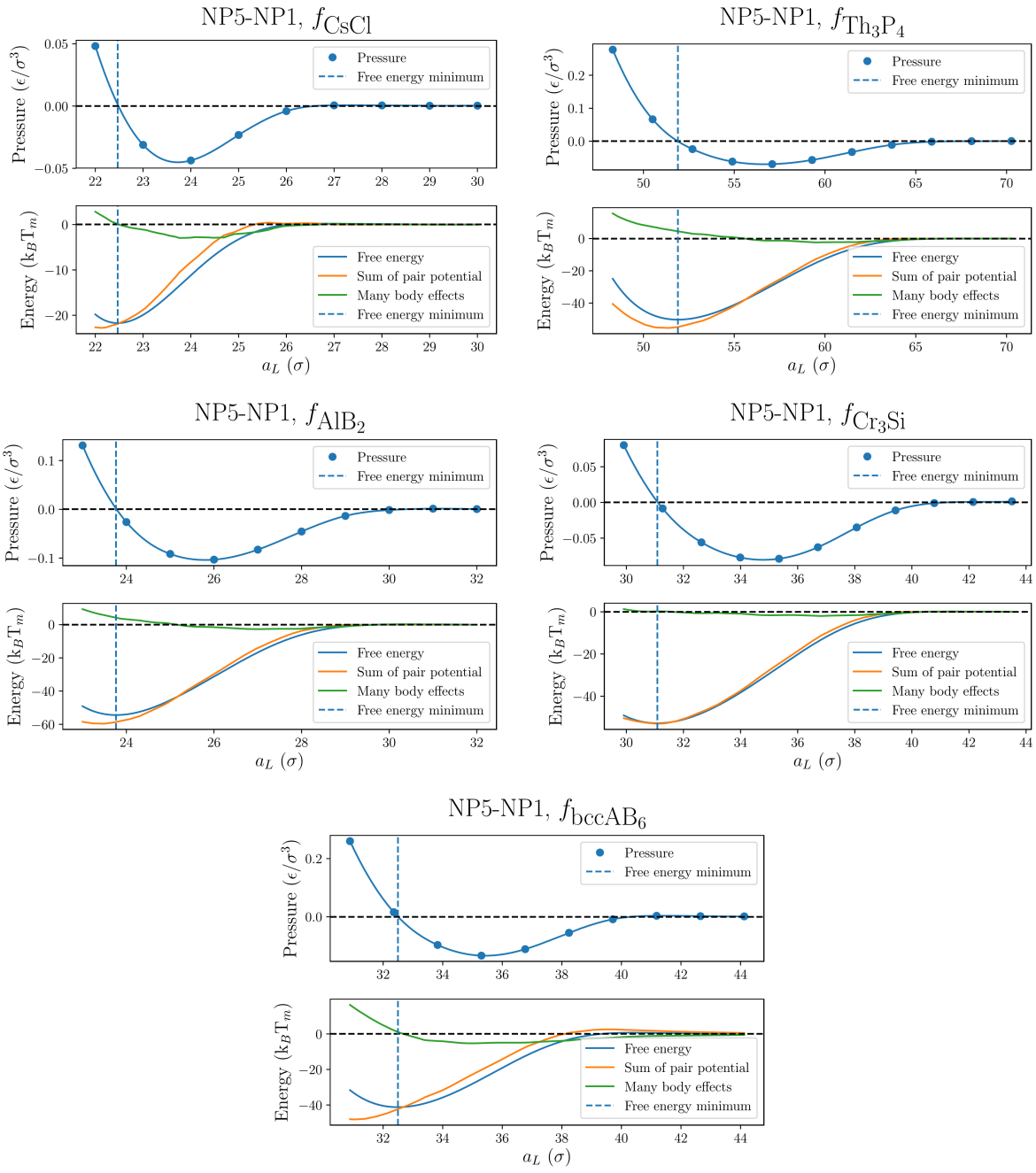

Figure S6: Pressure and free energy vs lattice constant for the BNSL CsCl, Th_3P_4, AlB_2, Cr_3Si and $bccAB_6$ with NP1 and NP5 normalized to the number of NPs within the unit cell.

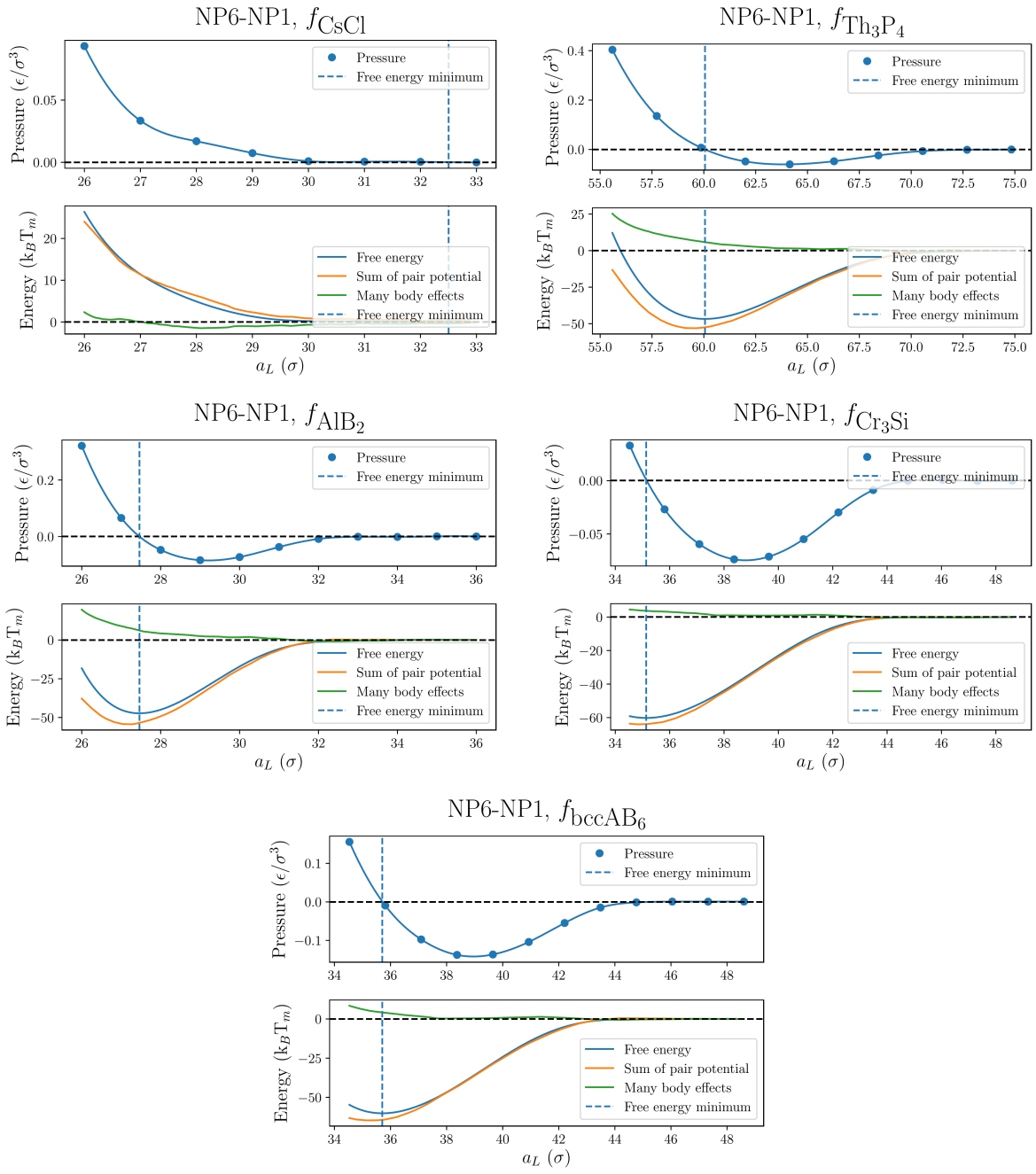

Figure S7: Pressure and free energy vs lattice constant for the BNSL CsCl, Th_3P_4, AlB_2, Cr_3Si and $bccAB_6$ with NP1 and NP6 normalized to the number of NPs within the unit cell.

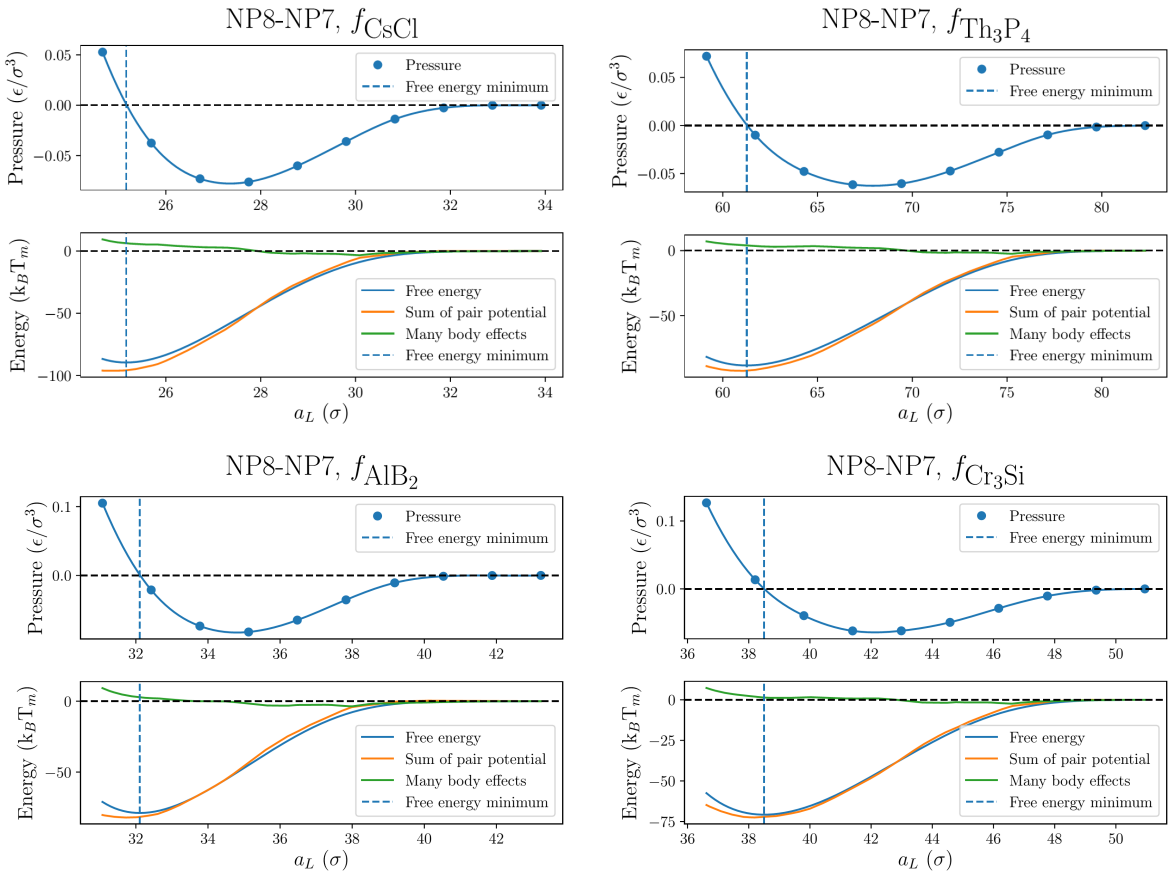

Figure S8: Pressure and free energy vs lattice constant for the BNSL CsCl, Th_3P_4, AlB_2, and Cr_3Si with NP7 and NP8 normalized to the number of NPs within the unit cell.

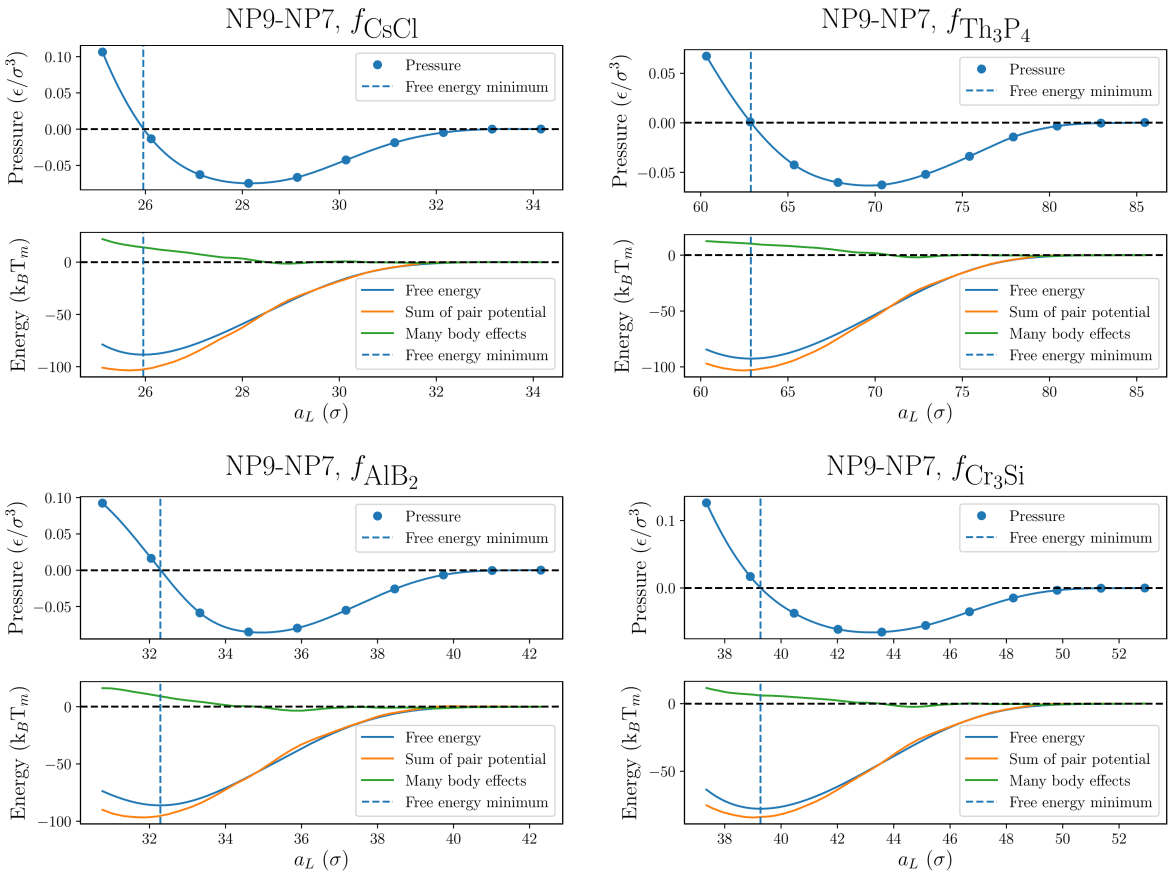

Figure S9: Pressure and free energy vs lattice constant for the BNSL CsCl, Th_3P_4, AlB_2, and Cr_3Si with NP7 and NP9 normalized to the number of NPs within the unit cell.

Tables Characterizing BNSL at the Free Energy Minimum

Table S6: Contributions of internal energy, $-T_m\Delta S$, free energy and the repulsive part, the average percent of hybridizations and lattice constants at the free energy minimum.

NP1-NP1 ($\gamma = 1.0$)	$\frac{U}{k_BT_m}$	$\frac{-\Delta S}{k_B}$	$\frac{F}{k_BT_m}$	f_r (%)	$\langle p_H \rangle$	$a_L(\sigma)$	OPM	OTM
CsCl	-223.6	193.18	-36.35	4.33	0.640	15.13	11.58	11.58
Th_3P_4	-210.6	183.11	-32.23	3.90	0.531	37.48	28.98	28.98
AlB_2	-171.4	153.55	-21.63	22.74	0.358	21.75	17.37	17.37
Cr_3Si	-137.0	120.74	-18.68	18.70	0.261	24.65	20.06	20.06
bccAB$_6$	0	0	0	100	0			

Table S7: Contributions of internal energy, $-T_m\Delta S$, free energy and the repulsive part, the average percent of hybridizations and lattice constants at the free energy minimum.

NP2-NP1 ($\gamma = 0.81$)	$\frac{\mathrm{U}}{k_B T_m}$	$\frac{-\Delta S}{k_B}$	$\frac{\mathrm{F}}{k_B T_m}$	f_r (%)	$\langle p_H \rangle$	$a_L(\sigma)$	OPM	OTM
CsCl	-270.8	232.93	-37.84	4.50	0.772	16.70	12.97	12.97
Th_3P_4	-283.1	244.95	-38.14	2.01	0.712	40.61	32.45	32.45
AlB_2	-270.6	236.48	-34.13	12.57	0.654	21.61	17.45	17.45
Cr_3Si	-227.9	198.60	-31.75	8.93	0.736	25.72	22.46	22.46
bccAB$_6$	0	0	0	100	0			

Table S8: Contributions of internal energy, $-T_m\Delta S$, free energy and the repulsive part, the average percent of hybridizations and lattice constants at the free energy minimum.

NP8-NP7 ($\gamma = 0.78$)	$\frac{\mathrm{U}}{k_B T_m}$	$\frac{-\Delta S}{k_B}$	$\frac{\mathrm{F}}{k_B T_m}$	f_r (%)	$\langle p_H \rangle$	$a_L(\sigma)$	OPM	OTM
CsCl	-691.8	602.15	-89.62	6.57	0.713	25.17	20.77	20.77
Th_3P_4	-723.3	634.97	-88.33	0.51	0.652	61.27	51.98	51.98
AlB_2	-690.5	611.57	-78.88	15.62	0.541	32.11	27.32	27.32
Cr_3Si	-600.3	529.51	-70.79	8.46	0.631	38.50	32.18	32.18
bccAB$_6$	0	0	0	100	0			

Table S9: Contributions of internal energy, $-T_m\Delta S$, free energy and the repulsive part, the average percent of hybridizations and lattice constants at the free energy minimum.

NP9-NP7 ($\gamma = 0.74$)	$\frac{\mathrm{U}}{k_B T_m}$	$\frac{-\Delta S}{k_B}$	$\frac{\mathrm{F}}{k_B T_m}$	f_r (%)	$\langle p_H \rangle$	$a_L(\sigma)$	OPM	OTM
CsCl	-699.3	610.87	-88.45	8.07	0.723	25.96	21.39	21.39
Th_3P_4	-749.9	657.3	-92.60	0.25	0.678	62.87	53.52	53.52
AlB_2	-735.9	649.70	-86.16	13.04	0.566	32.28	27.32	27.32
Cr_3Si	-649.6	571.85	-77.70	5.78	0.596	39.27	33.14	33.14
bccAB$_6$	0	0	0	100	0			

Table S10: Contributions of internal energy, $-T_m\Delta S$, free energy and the repulsive part, the average percent of hybridizations and lattice constants at the free energy minimum.

NP3-NP1 ($\gamma = 0.74$)	$\frac{\mathrm{U}}{k_BT_m}$	$\frac{-\Delta S}{k_B}$	$\frac{\mathrm{F}}{k_BT_m}$	f_r (%)	$\langle p_H \rangle$	$a_L(\sigma)$	OPM	OTM
CsCl	-277.3	238.05	-39.24	7.56	0.796	17.57	13.64	13.64
Th_3P_4	-300.8	259.4	-41.41	1.88	0.757	42.37	34.14	34.14
AlB_2	-308.1	268.32	-39.79	10.60	0.659	21.67	16.96	16.96
Cr_3Si	-268.6	233.47	-35.09	7.88	0.691	26.43	21.14	19.05
bccAB$_6$	0	0	0	100	0			

Table S11: Contributions of internal energy, $-T_m\Delta S$, free energy and the repulsive part, the average percent of hybridizations and lattice constants at the free energy minimum.

NP4-NP1 ($\gamma = 0.68$)	$\frac{\mathrm{U}}{k_BT_m}$	$\frac{-\Delta S}{k_B}$	$\frac{\mathrm{F}}{k_BT_m}$	f_r (%)	$\langle p_H \rangle$	$a_L(\sigma)$	OPM	OTM
CsCl	-278.5	238.99	-39.46	12.26	0.801	18.51	14.74	14.74
Th_3P_4	-312.7	268.22	-44.46	3.86	0.790	44.22	35.78	35.78
AlB_2	-334.7	290.20	-44.54	10.41	0.718	21.81	17.36	17.36
Cr_3Si	-305.4	265.25	-40.12	3.82	0.637	27.24	22.15	20.05
bccAB$_6$	-0.1	0.06	-0.04	100	0			

Table S12: Contributions of internal energy, $-T_m\Delta S$, free energy and the repulsive part, the average percent of hybridizations and lattice constants at the free energy minimum.

NP5-NP1 ($\gamma = 0.52$)	$\frac{\mathrm{U}}{k_BT_m}$	$\frac{-\Delta S}{k_B}$	$\frac{\mathrm{F}}{k_BT_m}$	f_r (%)	$\langle p_H \rangle$	$a_L(\sigma)$	OPM	OTM
CsCl	-241.9	220.13	-21.72	30.82	0.701	22.47	19.19	19.19
Th_3P_4	-327.1	276.79	-50.28	4.42	0.831	51.90	42.21	42.21
AlB_2	-364.5	310.01	-54.45	8.49	0.788	23.77	19.19	19.19
Cr_3Si	-381.8	329.01	-52.83	0.51	0.729	31.09	26.14	22.18
bccAB$_6$	-354.6	313.39	-39.49	18.90	0.649	32.50	28.37	25.23

Table S13: Contributions of internal energy, $-T_m\Delta S$, free energy and the repulsive part, the average percent of hybridizations and lattice constants at the free energy minimum.

NP6-NP1 ($\gamma = 0.43$)	$\frac{\mathrm{U}}{k_BT_m}$	$\frac{-\Delta S}{k_B}$	$\frac{\mathrm{F}}{k_BT_m}$	f_r (%)	$\langle p_H \rangle$	$a_L(\sigma)$	OPM	OTM
CsCl	0	0	0	100	0	32.50	23.50	23.50
Th_3P_4	-310.9	264.13	-46.72	12.19	0.800	60.05	50.25	50.25
AlB_2	-346.1	298.83	-47.28	16.33	0.758	27.47	23.50	23.50
Cr_3Si	-407.1	346.90	-60.24	0.76	0.784	35.12	29.99	27.09
bccAB$_6$	-431.5	371.31	-60.17	9.67	0.722	35.71	29.99	28.53

Effects of Rigidity

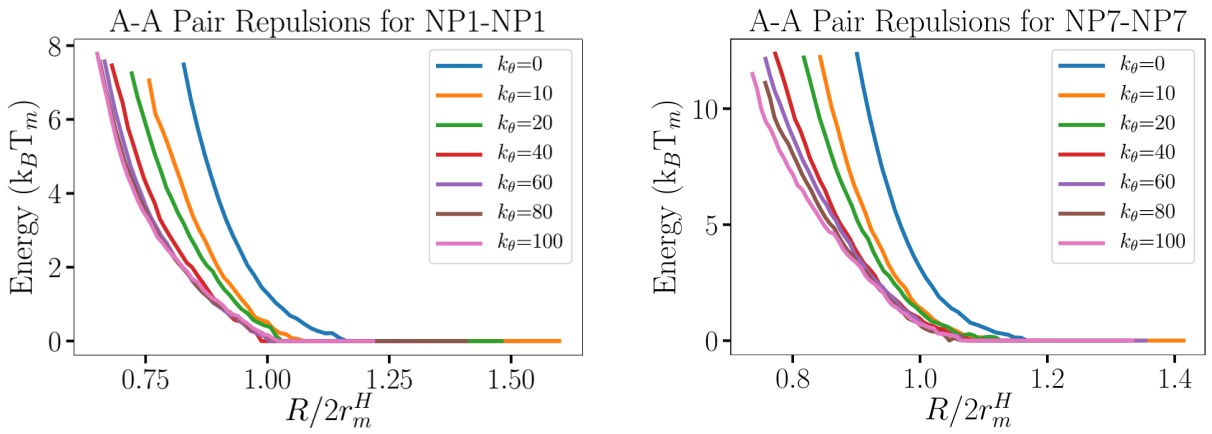

(a) (b)

Figure S10: Pair repulsions as a function of the spring parameter k_θ of the harmonic angle potential for (a) NP1 - NP1 and (b) NP7 - NP7.

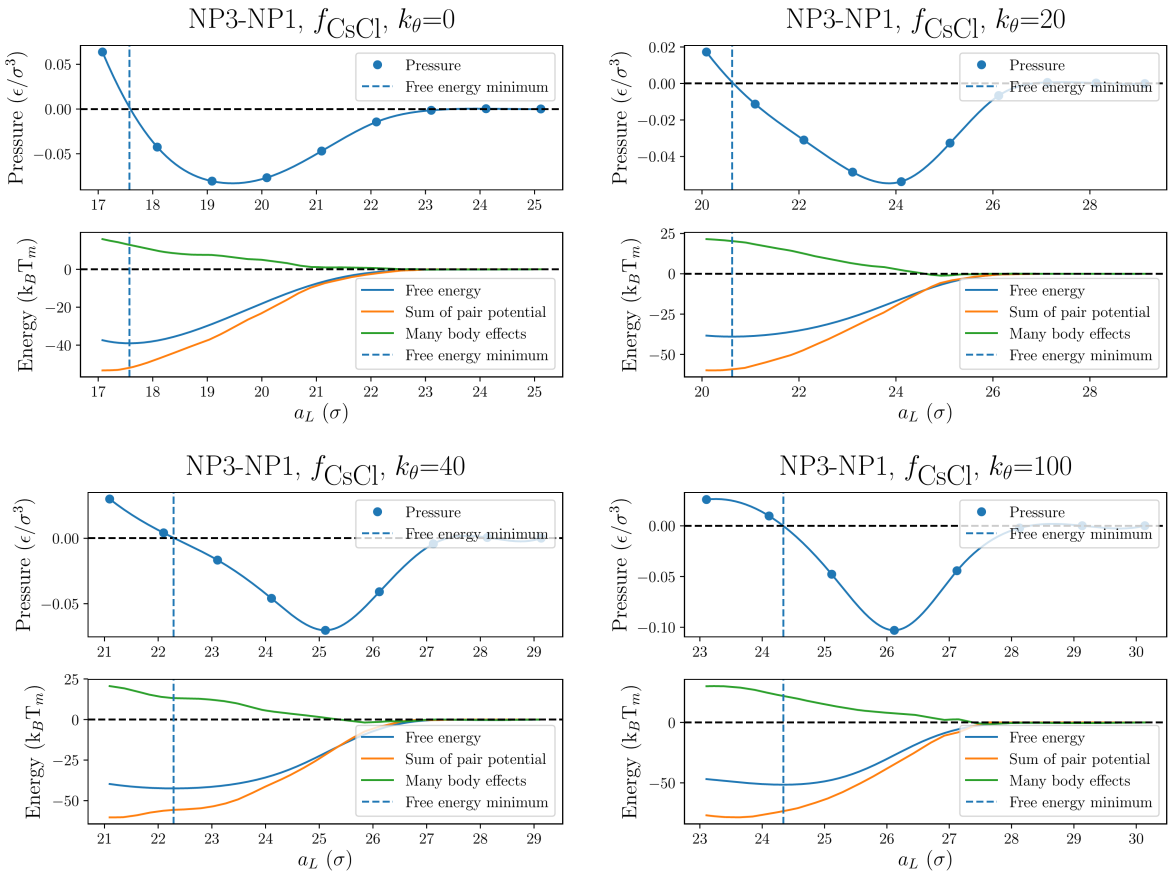

Figure S11: Pressure and free energy vs lattice constant for the BNSL CsCl with NP1 and NP3 under the different values of the spring parameter k_θ of the harmonic angle potential normalized to the number of NPs within the unit cell.

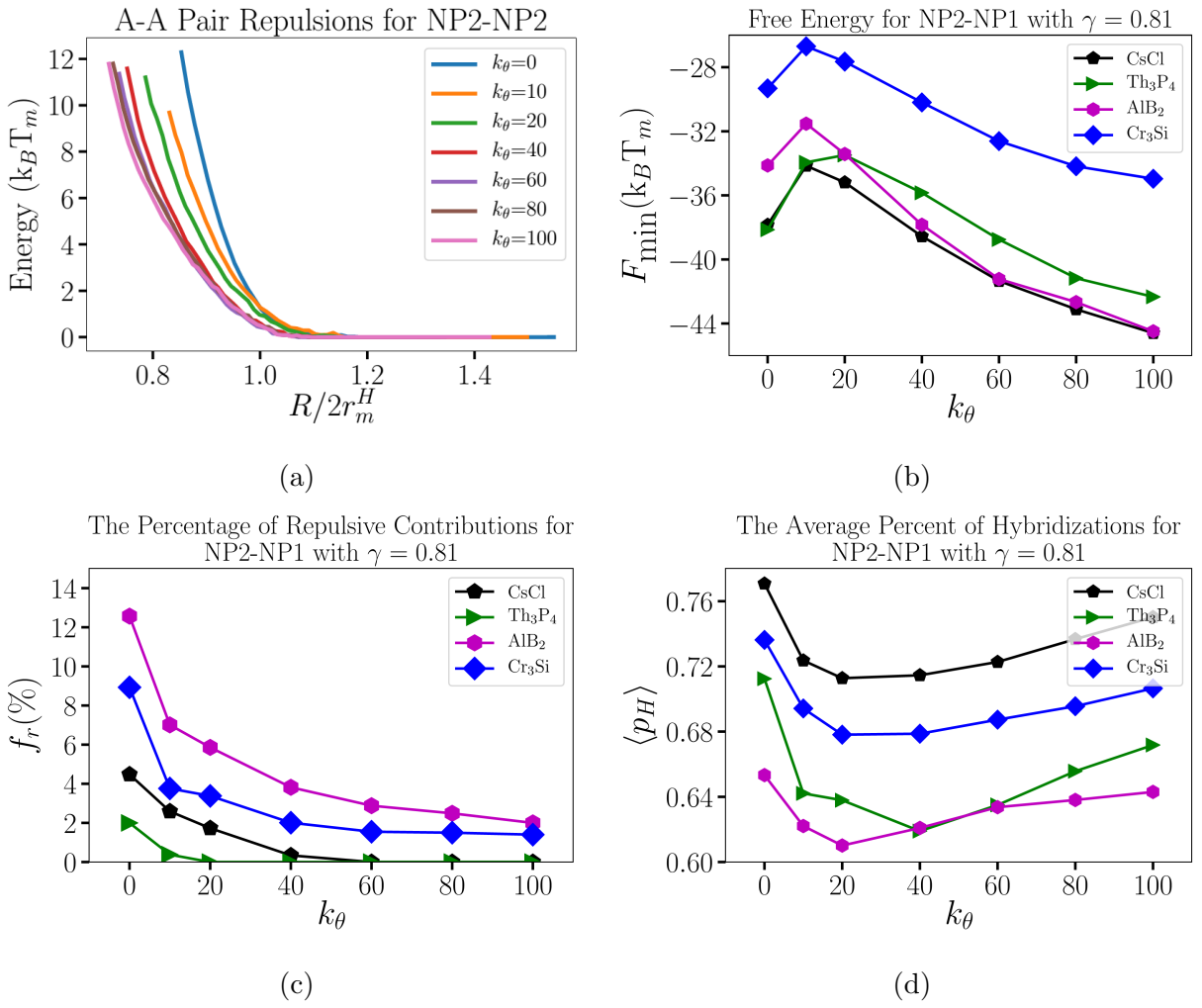

Figure S12: The effect of the spring parameter k_θ of the harmonic angle potential on (a) potential of mean force (NP2-NP2), (b) free energies, (c) the repulsive fraction f_r (see Eq. 17) and (d) the average percent of hybridizations $\langle p_H \rangle$ for CsCl, Th_3P_4, AlB_2 and Cr_3Si with $\gamma = 0.74$ (NP2 - NP1), see Table 2 for detailed values. All values are for $\frac{\varepsilon_{AB}}{k_BT_m} = 13.0$.

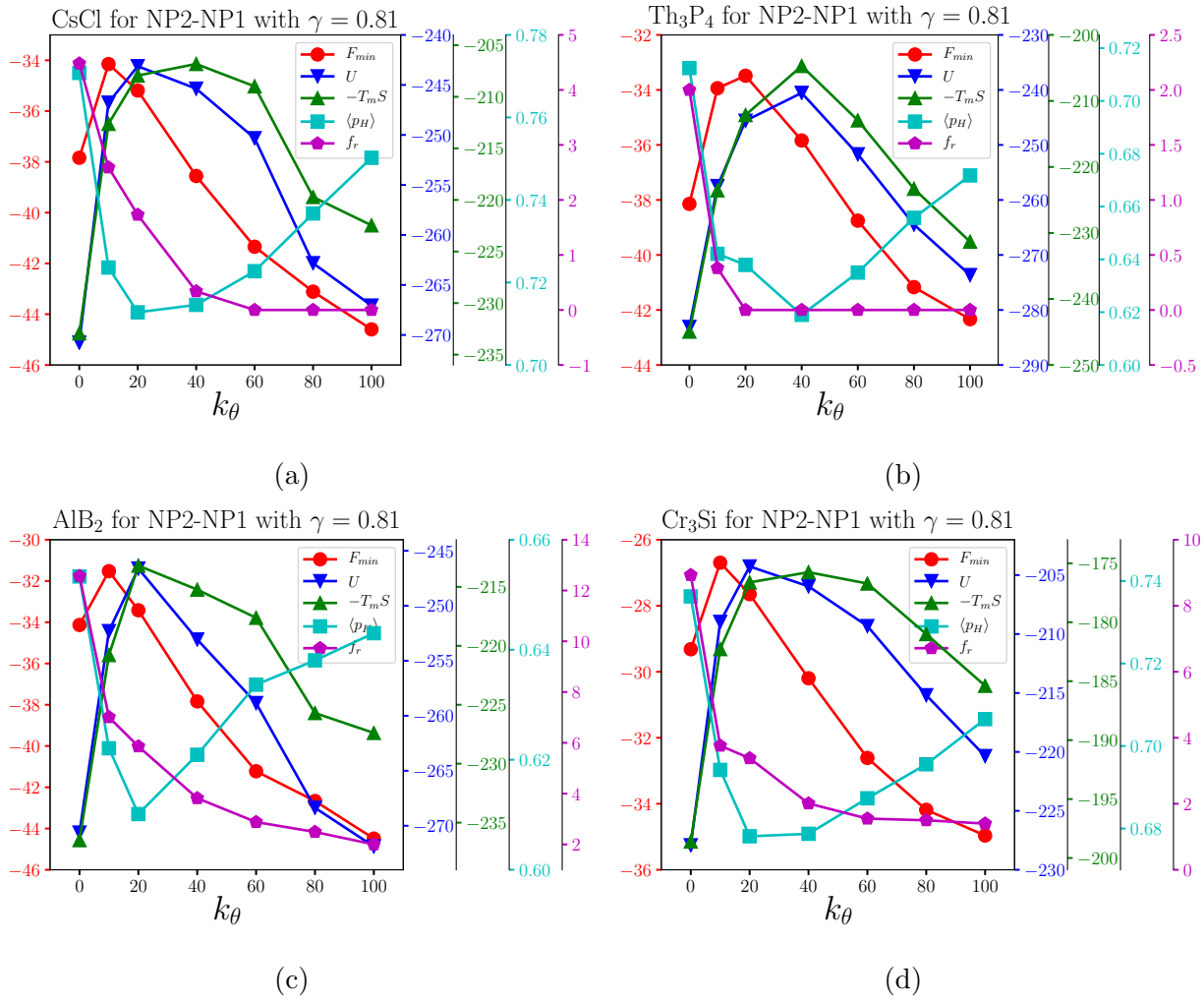

Figure S13: The variations of free energies, internal energies, entropy, the average percent of hybridizations $\langle p_H \rangle$ and the repulsive fraction f_r with the spring parameter k_θ of the harmonic angle potential for (a) CsCl, (b) Th_3P_4, (c) AlB_2 and (d) Cr_3Si with $\gamma = 0.81$ (NP2 - NP1), see Table 2 for detailed values. All values are for $\frac{\varepsilon_{AB}}{k_B T_m} = 13.0$. The units for the free energies, internal energies and -T_mS are all $k_B T_m$.

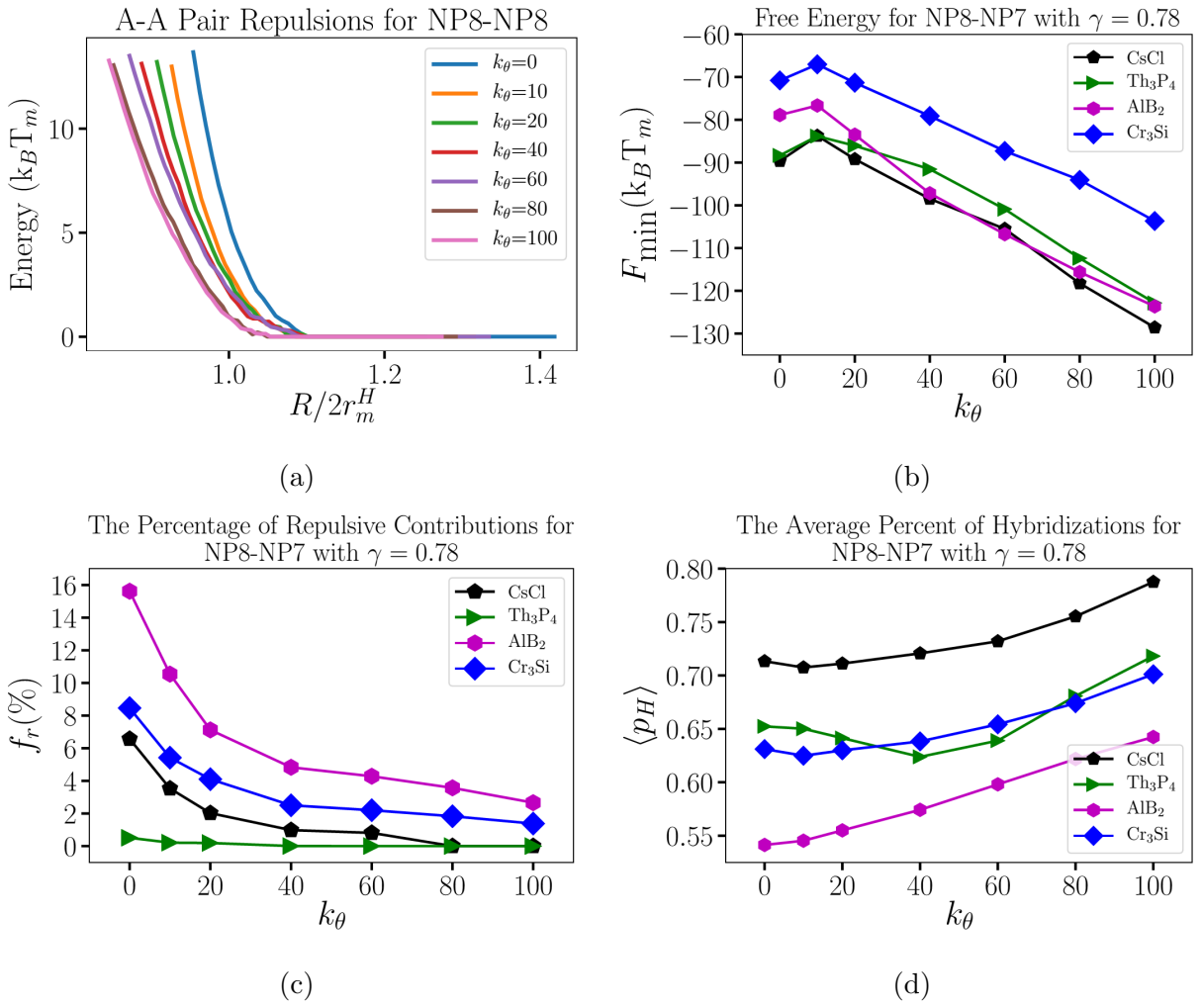

Figure S14: The effect of the spring parameter k_θ of the harmonic angle potential on (a) potential of mean force (NP9-NP9), (b) free energies, (c) the repulsive fraction f_r (see Eq. 17) and (d) the average percent of hybridizations $\langle p_H \rangle$ for CsCl, Th_3P_4, AlB_2 and Cr_3Si with $\gamma = 0.78$ (NP8 - NP7), see Table 2 for detailed values. All values are for $\frac{\varepsilon_{AB}}{k_BT_m} = 13.0$.

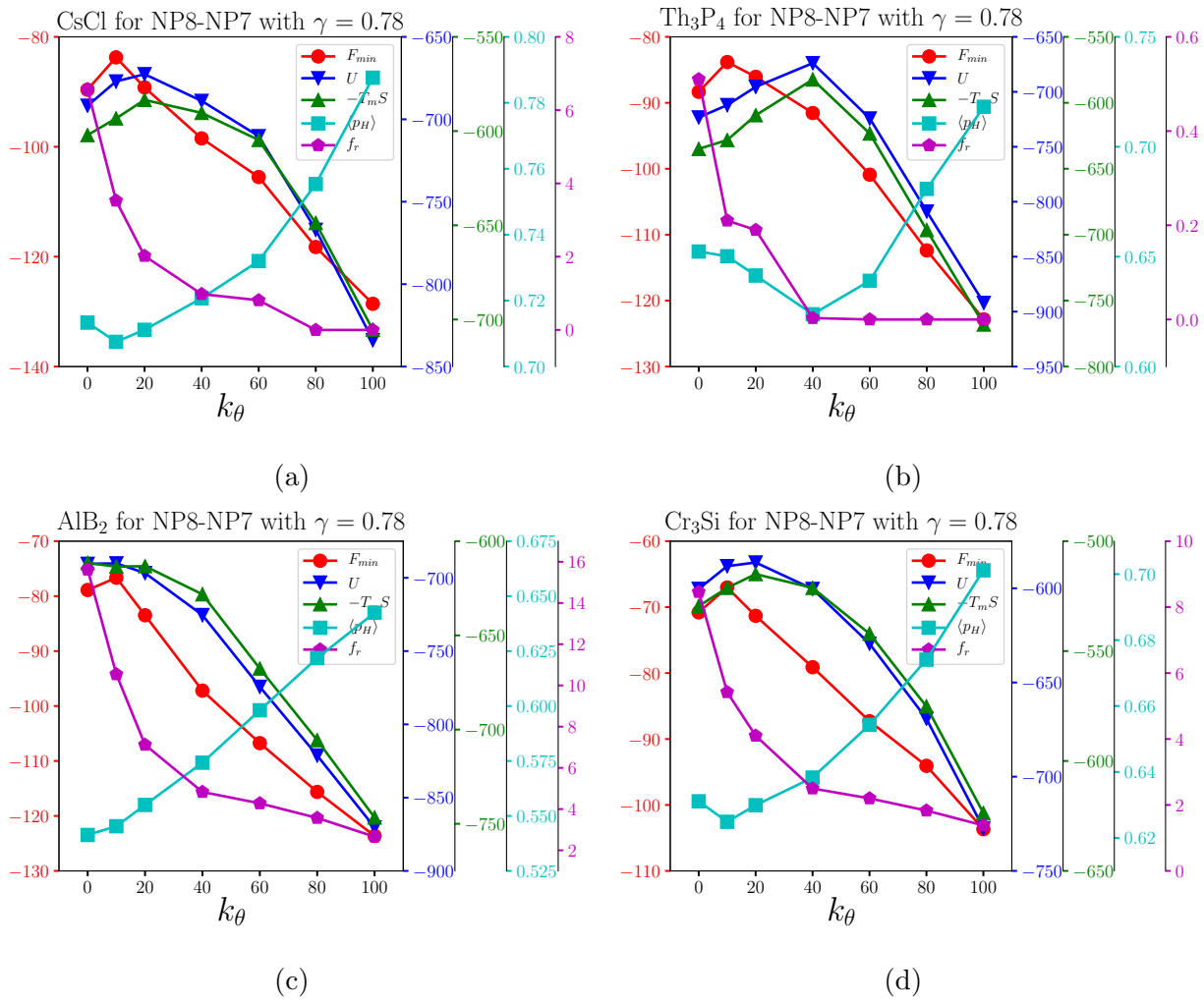

Figure S15: Free energies, internal energies, entropy, the average percent of hybridizations $\langle p_H \rangle$ and the repulsive fraction f_r vs the spring parameter k_θ of the harmonic angle potential for (a) CsCl, (b) Th_3P_4, (c) AlB_2 and (d) Cr_3Si with $\gamma = 0.78$ (NP8 - NP7), see Table 2 for detailed values. All values are for $\frac{\varepsilon_{AB}}{k_B T_m} = 13.0$. The units for the free energies, internal energies and -T_mS are all $k_B T_m$.

Comparison to Experiment

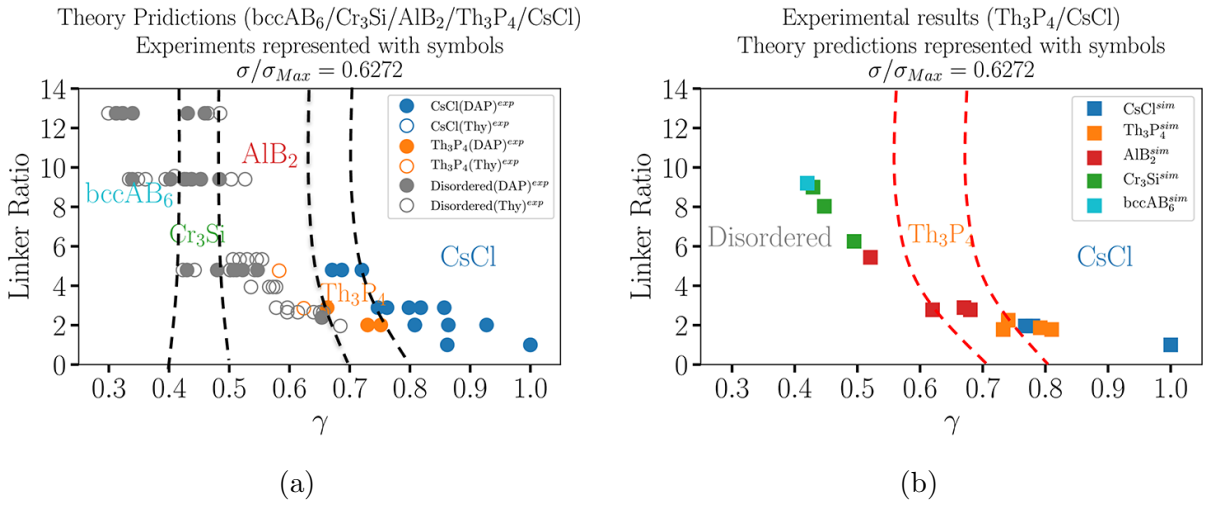

Figure S16: (a)The theoretical and (b) experimental phase diagrams as a function of the hard sphere radius ratio with $\sigma_g/\sigma_{g,Max} = 0.6272$ and the PS coverage ratios (large to small NCT), where the black dashed lines are phase boundaries. The circle symbols are the experimental results and the squares indicate our simulated values. DAP and Thy in brackets indicate that the NCTs with DAP or Thy are A particles.

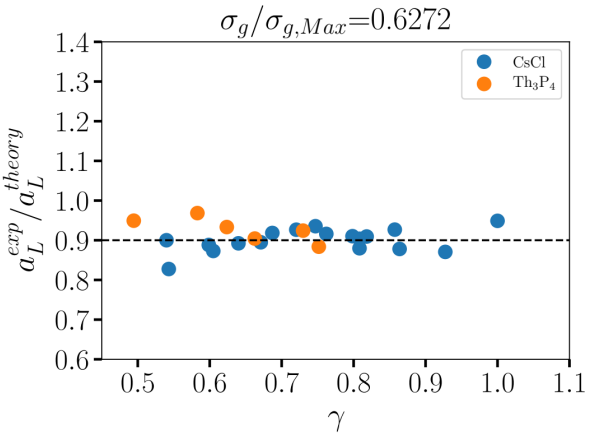

Figure S17: The comparison of the measured lattice constant and the predicted values of the OPM formula by assuming $\sigma_g/\sigma_{g,Max} = 0.6272$.

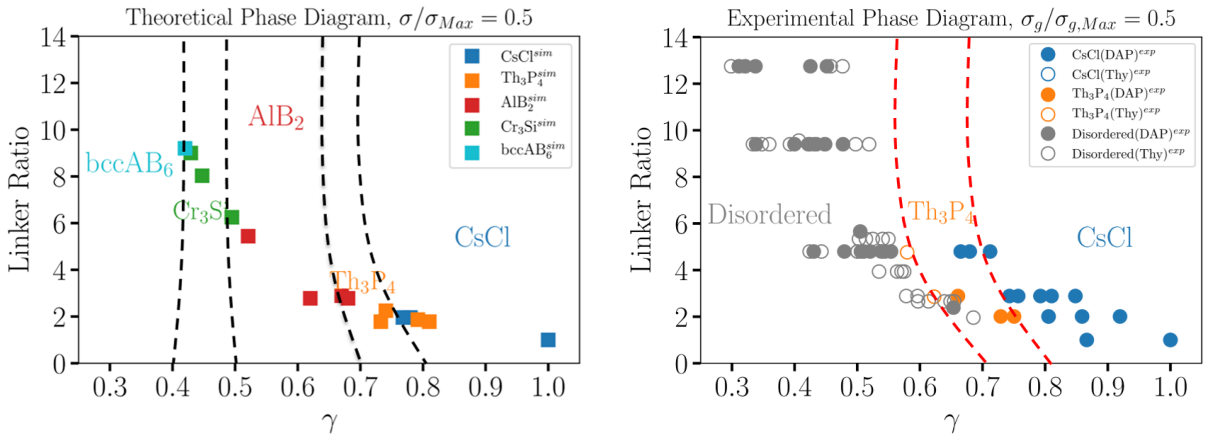

(a) (b)

Figure S18: (a)The theoretical and (b) experimental phase diagrams as a function of the hard sphere radius ratio with $\sigma_g/\sigma_{g,Max} = 0.5$ and the PS coverage ratios (large to small NCT), which are determined by the corresponding the simulated and experimental data points. DAP and Thy in brackets indicate that the NCTs with DAP or Thy are A particles.

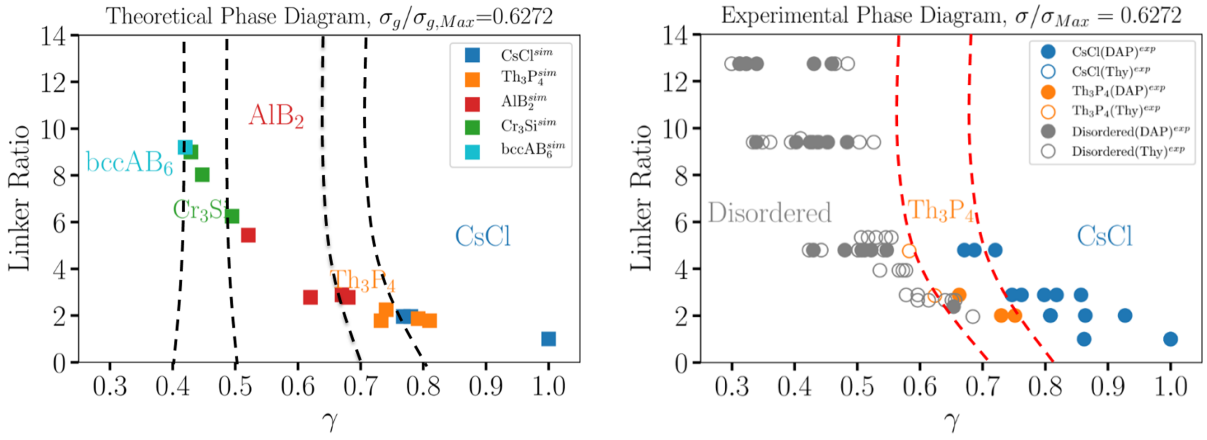

(a) (b)

Figure S19: (a)The theoretical and (b) experimental phase diagrams as a function of the hard sphere radius ratio with $\sigma_g/\sigma_{g,Max} = 0.6272$ and the PS coverage ratios (large to small NCT), which are determined by the corresponding the simulated and experimental data points. DAP and Thy in brackets indicate that the NCTs with DAP or Thy are A particles.

Experimental Section

Table S14: Molecular weight (MW) and dispersities of the polymers used in our experiments.

Polymer Name	MW(kDa)	Dispersity
6k DAP	6.4	1.08
6k Thy	6.5	1.09
9k DAP	8.7	1.17
9k Thy	9.5	1.10
11k DAP	11.3	1.04
11k Thy	11.4	1.04
14k DAP	14.3	1.27
14k Thy	14.0	1.06
16k DAP	16.1	1.35
16k Thy	15.9	1.03
18k DAP	17.8	1.09
18k Thy	18.5	1.17

Table S15: Size and dispersities of the gold nanoparticles used in our experiments.

Diameter (nm)	Relative Standard Deviation (%)	Centrifuge Protocol
12.1	8.8	9,000 RPM, 50 minutes
15.6	8.1	7,000 RPM, 50 minutes
18.7	9.8	7,000 RPM, 40 minutes
26.5	11.1	7,000 RPM, 30 minutes
37.1	10.6	2.500 RPM, 25 minutes

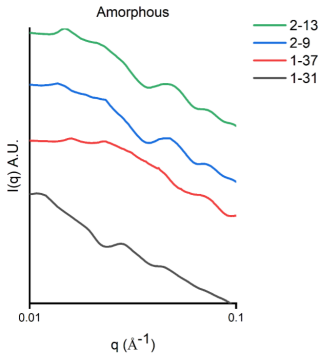

Figure S20: SAXS curves for some typical samples with amorphous structure.

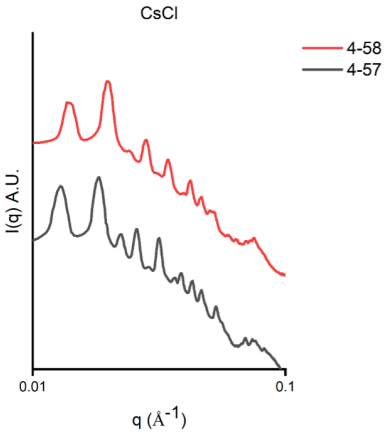

Figure S21: SAXS curves for some typical samples with the CsCl BNSL.

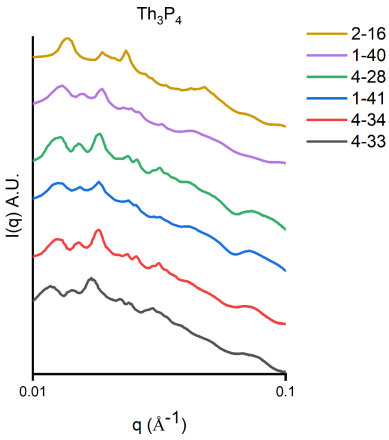

Figure S22: SAXS curves for some typical samples with the Th_3P_4 BNSL.

Effect of solvent quality

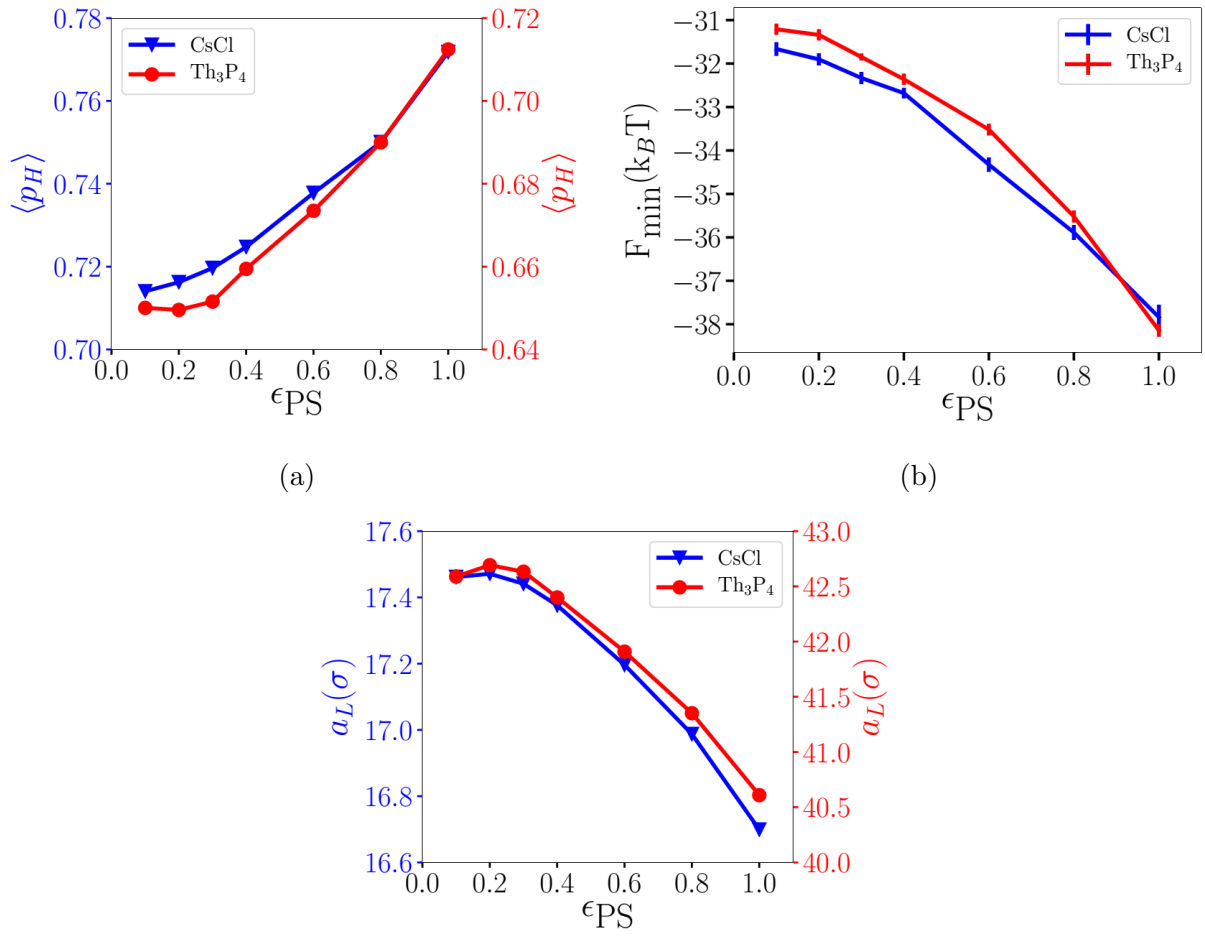

Figure S23: (a)The average percent of hybridizations as a function of ϵ_{PS} for the CsCl and Th_3P_4 lattices with NP1 and NP2; (b) The minimum of the free energy F_{min} and (d) the corresponding lattice constant a_L varies with ϵ_{PS} for the CsCl and Th_3P_4 lattices.

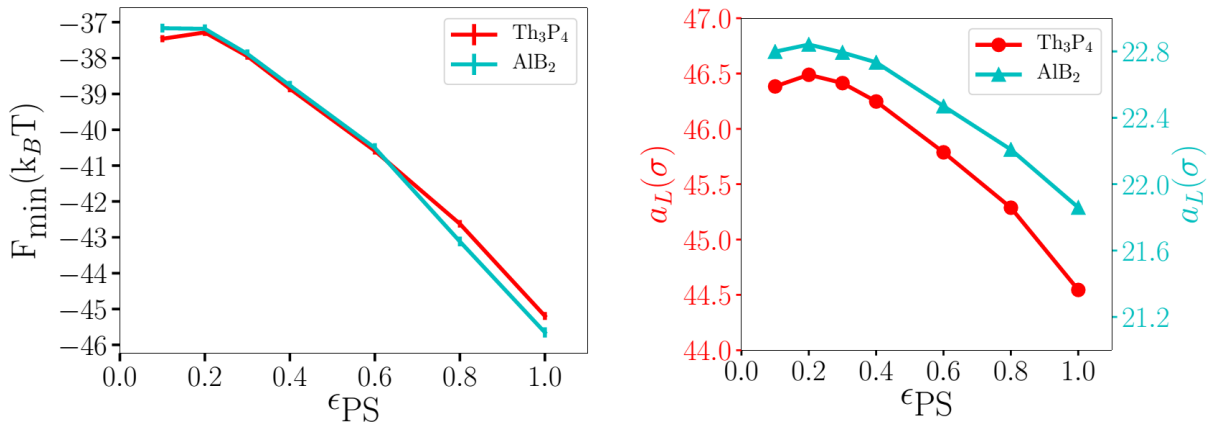

(a) (b)

Figure S24: (a)The average percent of hybridizations as a function of ϵ_{PS} for the CsCl and Th_3P_4 lattices with NP1 and 25.5nm(8k) where $\gamma = 0.67$; (b) The minimum of the free energy F_{min} and (d) the corresponding lattice constant a_L varies with ϵ_{PS} for the CsCl and Th_3P_4 lattices with 15nm(8k) and 25.5nm(8k) where $\gamma = 0.67$.

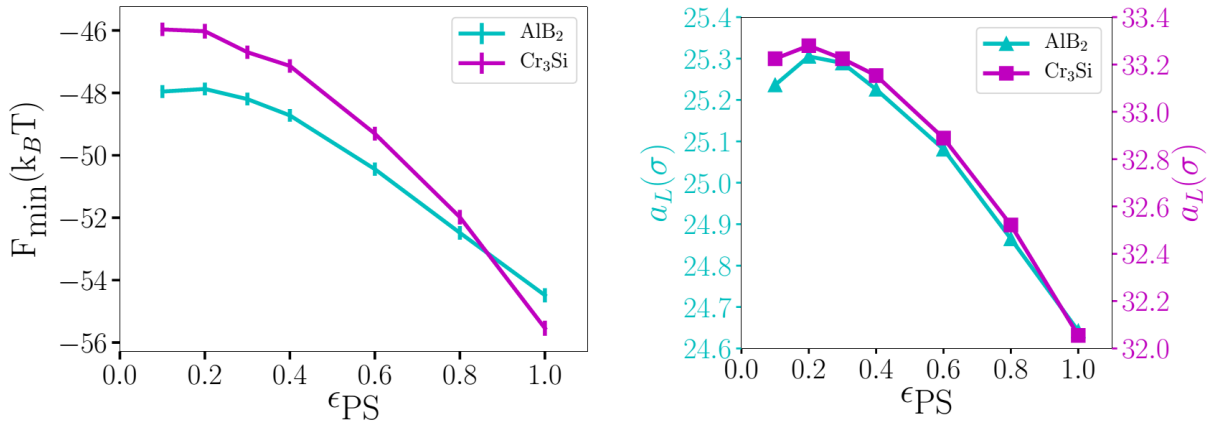

(a) (b)

Figure S25: (a) The minimum of the free energy F_{min} and (b) the corresponding lattice constant a_L varies with ϵ_{PS} for AlB_2 and Cr_3Si lattices with 15nm(8k) and 37.5nm(8k) where $\gamma = 0.49$.

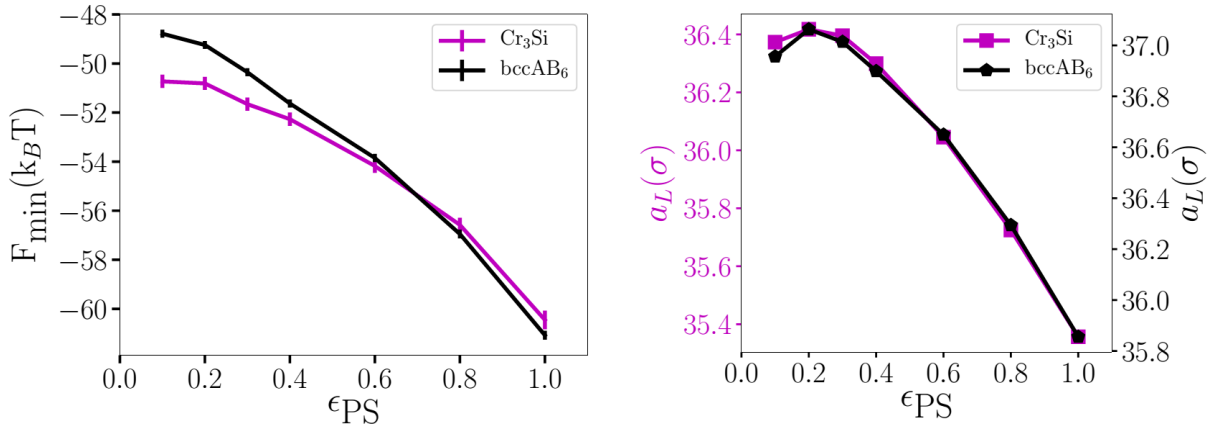

(a) (b)

Figure S26: (a) The minimum of the free energy F_{min} and (b) the corresponding lattice constant a_L varies with ϵ_{PS} for Cr_3Si and $bccAB_6$ lattices with 15nm(8k) and 46nm(8k) where $\gamma = 0.42$.